CHEMISTRY
A EUROPEAN JOURNAL

DOI: 10.1002/chem.200800591

The Extended View on the Empty $C_2(3)$-C_{82} Fullerene: Isolation, Spectroscopic, Electrochemical, and Spectroelectrochemical Characterization and DFT Calculations

Michal Zalibera,[a, b] Alexey A. Popov,[a, c] Martin Kalbac,[a, d] Peter Rapta,[a, b] and Lothar Dunsch*[a]

Abstract: An extended study of the spectroscopic and redox properties of the C_{82} fullerene is presented. Among the nine isolated-pentagon-rule (IPR) isomers of the C_{82} fullerene the $C_{82}(3)$ isomer with C_2 symmetry is the only stable, empty fullerene structure formed in the arc burning process that can be isolated in an isomerically pure form. Here, its formation and isolation are described and its structure is confirmed by experimental spectroscopic studies as well as time-dependent DFT calculations. The electrochemistry of the $C_{82}(3)$ isomer is studied in detail by cyclic voltammetry and spectroelectrochemistry. The anionic species of C_{82} with the charge ranging from C_{82}^{-} to C_{82}^{4-} were successively generated in *o*-dichlorobenzene solution at room temperature and characterized by in situ ESR and visible/near-infrared (Vis/NIR) spectroscopy. The data give new insights into the charged states of the $C_{82}(3)$ fullerene.

Keywords: electrochemistry · EPR spectroscopy · fullerenes · NMR spectroscopy · spectroelectrochemistry · vibrational spectroscopy

Introduction

In contrast to the most abundant (and the most studied) empty fullerenes C_{60} and C_{70}, which exist only in a single isomeric form, nine isolated-pentagon-rule (IPR) isomers are proposed for the C_{82} fullerene.[1] The cage isomers of the same fullerene usually exhibit substantial differences in their electronic structure and, consequently, in their physicochemical properties. Only a few isomers of C_{82} can be generated in significant abundance in the fullerene-production process. In contrast to these empty fullerenes, the most abundant metallo- and multimetallofullerenes formed by the Krätschmer–Huffman fullerene synthesis were found to have either C_{82} or C_{84} cages.[2–4] They have attracted much attention due to their unique properties resulting from the charge transfer between the encapsulated metal atom and the fullerene cage as well as due to the properties of the encapsulated species. The C_{82}-based endohedral metallofullerenes have been widely studied both experimentally and theoretically. In general, the encapsulated metal donates its valence electrons to the C_{82} cage forming a nondissociating salt consisting of a negatively charged cage and positively charged metal ion (or metal cluster) inside the cage. The number of transferred electrons depends on the nature of the encapsulated species, and, hence, the cage isomerism in C_{82}-based metallofullerenes varies depending on this factor. Therefore, it is of high interest to have detailed studies of negatively charged, empty C_{82} isomers.

Most M@C_{82} metallofullerenes consist of the $C_{2v}(9)$-C_{82} carbon cage.[5] However, there are several examples in the M@C_{82} endohedral family in which the C_{82} host cage exhib-

[a] M. Zalibera, Dr. A. A. Popov, Dr. M. Kalbac, Dr. P. Rapta, Prof. Dr. L. Dunsch
Department of Electrochemistry and Conducting Polymers
Leibniz Institute for Solid State and Materials Research
01069 Dresden (Germany)
Fax: (+49) 351-465-9811
E-mail: L.Dunsch@ifw-dresden.de

[b] M. Zalibera, Dr. P. Rapta
Department of Physical Chemistry
Faculty of Chemical and Food Technology
Slovak University of Technology
81237 Bratislava (Slovak Republic)

[c] Dr. A. A. Popov
Chemistry Department, Moscow State University
Moscow 119992 (Russia)

[d] Dr. M. Kalbac
J. Heyrovsky Institute of Physical Chemistry
18223 Prague (Czech Republic)

Supporting information for this article is available on the WWW under http://dx.doi.org/10.1002/chem.200800591.

its different isomeric structures, even for the same encapsulated metal. For instance, three different isomers have been identified for Tm@C_{82}.[6,7] Thus, a variety of C_{82} cages with different symmetry and different charge on the host cage were suggested or identified for M_n@C_{82} metallofullerenes pointing to the complexity of the exact attribution of the C_{82} fullerene host cage symmetry, its charge, and their relationship in endohedral metallofullerenes.

ESR and visible/near-infrared (Vis/NIR) spectra of charged fullerenes are very important in the characterization of the corresponding fulleride anions and fullerene cations.[8,9] However, ESR and Vis/NIR studies on the charged C_{82} cage are quite rare, and there are no systematic investigations on the negatively charged states of this prominent fullerene cage. Recently, we succeeded in preparing macroscopic quantities of the pure $C_2(3)$-C_{82} fullerene isomer.[10] In this contribution we report the isolation and detailed spectroscopic, spectroelectrochemical, and theoretical characterization of the $C_2(3)$-C_{82} fullerene isomer in its neutral and charged states.

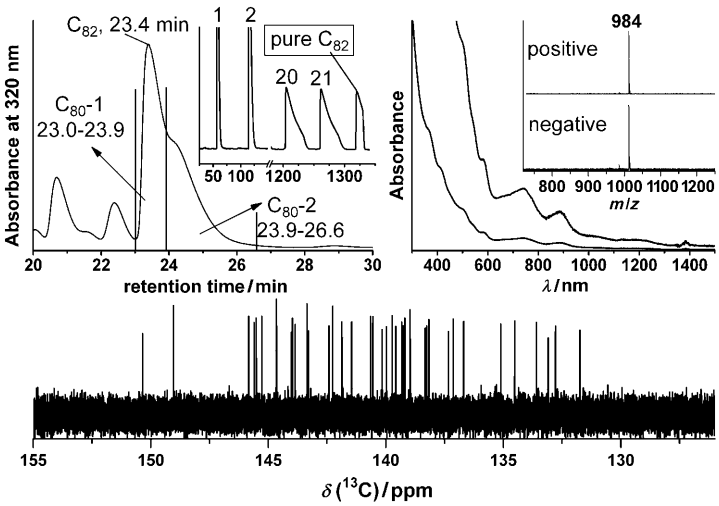

Figure 1. Top Left: HPLC of the fraction used to separate $C_2(3)$-C_{82}; inset: recycling HPLC trace showing the two first (1, 2) and two last cycles (20, 21) as well as the final cycle, indicating the pure $C_2(3)$-C_{82} sample. Top right: UV/Vis/NIR absorption spectrum of $C_2(3)$-C_{82} in o-DCB; inset shows the LDI mass spectra of the sample measured in positive and negative modes. Bottom: ^{13}C NMR spectrum of $C_2(3)$-C_{82} (CS_2 solution).

Results and Discussion

Preparation and separation: As a by-product in the fullerene synthesis, the fullerene C_{82} is available only through an extensive separation procedure. Despite the fact that the larger C_{84} cage is the third most abundant fullerene (next to C_{60} and C_{70}) in the arc synthesis according to Krätschmer and Huffman, the total amount of C_{82} is so small that it is not detectable in the separation procedure by a standard UV/Vis detector cell in a HPLC system. Although it should be considered as an "impurity," it is well worth the separation, which, however, turns out to be rather extensive. We used two fractions of the soot for the production of endohedral fullerenes (preferably for lanthanum, but also for cerium, yttrium and samarium) containing as the main product C_{80} and C_{84}, respectively. Three-step HPLC separation by using several columns was necessary to achieve the full separation of the isomer. The HPLC chromatograms from the first stage and the recycling (inset) are shown in Figure 1 (top left). The purity of the sample was checked by mass spectrometry (Figure 1, top right, inset) and no contamination by higher or lower cages was observed after the final purification step.

^{13}C NMR spectroscopy: The ^{13}C NMR spectrum of the C_{82} fullerene sample in CS_2 (Figure 1, bottom) consists of 41 lines of nearly equal intensity indicating C_2 symmetry (41 × 2 C) in the C_{82} isomer. The chemical shifts of the NMR lines are identical with those observed by Kikuchi et al.[11,12] for the main C_{82} isomer. However, in addition to these 41 strong lines the authors of reference [11] detected 29 lines with moderate intensity and some other lines with weaker intensity in the ^{13}C NMR spectrum of their sample and interpreted them as the presence of two minor C_{82} isomers with C_{2v} and C_{3v} symmetries. In the supporting information of a more recent report (reference [13]), the ^{13}C NMR spectrum of a C_{82} sample with a significantly improved isomeric purity was presented, but some minor lines were detected also in this case. These lines are evidently absent in the spectrum of our sample and its purity with respect to other fullerene cage sizes was also proved by laser desorption ionization time-of-fight mass spectroscopic (LDI-TOF MS) measurements (Figure 1, top right, inset). Note that the exact isomeric structure of C_{82} cannot be unambiguously assigned based on a simple one-dimensional ^{13}C NMR experiment as three of the nine IPR-abiding isomers possess C_2 symmetry that would lead to the 41 line pattern in the NMR spectra. The 2D INADEQUATE experiment could answer the question; however, a ^{13}C-enriched sample would be necessary for an effective measurement. Sun and Kertesz[14] performed the theoretical calculation of the NMR spectra of all nine IPR isomers of the C_{82} fullerene and reported the $C_2(3)$-C_{82}[1] isomer as the best candidate for the main C_2 isomer. This was confirmed very recently by Gao et al. who calculated the ultraviolet photoelectron spectra (UPS) of C_{82} isomers using hybrid density functional theory.[15]

UV/Vis/NIR spectroscopy: The UV/Vis/NIR spectrum of the C_2-C_{82} isomer in 1,2-dichlorobenzene (*o*-DCB) with major absorption bands at 1180, 880, 743, 583 nm, a strong absorption in the UV range and a spectral onset around 1315 nm (Figure 1, top right) is identical to that observed by Fujitsuka et al.[13] in benzonitrile and by Kikuchi et al.[12] in benzene. Absorption patterns of fullerenes in the visible range are mainly due to the $\pi \rightarrow \pi^*$ excitations and show remarkable structural sensitivity. Bauernschmitt et al.[16] reported that time-dependent (TD) DFT calculations provide reliable predictions of the excitation energies and absorption

intensities (oscillator strengths) of fullerenes in the visible range. We employed this approach to confirm the isomeric structure of the sample studied in this work. Figure 2 compares the experimental spectrum of the C_2-C_{82} fullerene to the spectra simulated for $C_2(1)$, $C_2(3)$, and $C_2(5)$-C_{82} isomers. The spectrum calculated for $C_2(3)$-C_{82} provides a very good match to the experimental data, while the spectra of the other isomers do not (note that TD-DFT systematically underestimates the excitation energies, and the computed spectrum was uniformly shifted by 0.3 eV to the higher energy range). Hence, this is an additional confirmation of the $C_2(3)$-C_{82} molecular structure of the major C_{82} isomer. In fact, the agreement between experimental and calculated spectra is so good that the assignment of individual bands in the experimental spectrum (marked A–H in Figure 2) becomes possible and is provided in Table 1.

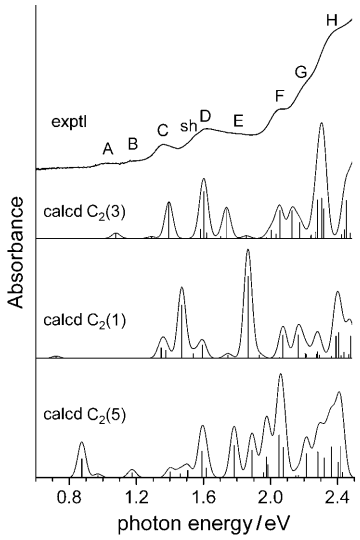

Figure 2. Experimental absorption spectrum of C_2-C_{82} in oDCB and the results of the TD-DFT calculations for $C_2(1)$, $C_2(3)$, and $C_2(5)$ isomers.

Table 1. Experimental excitation energies (E, eV) in $C_2(3)$-C_{82} and their assignment based on TD-DFT calculations.

band	Experimental E [eV]	$S_0 \rightarrow S_n$ [a]	Calculated E [eV]	f [b]	Leading configurations [%] [c]
A	1.04	$S_0 \rightarrow S_1$	0.804	0.0009	246→247 (100)
B	1.21	$S_0 \rightarrow S_2$	1.027	0.0003	245→247 (100)
C	1.40	$S_0 \rightarrow S_3$	1.136	0.0060	246→248 (97)
sh	1.60	$S_0 \rightarrow S_4$	1.334	0.0016	244→247 (97)
D	1.67	$S_0 \rightarrow S_5$	1.356	0.0079	245→248 (96)
E	1.88	$S_0 \rightarrow S_8$	1.498	0.0049	242→247 (97)
F	2.13	$S_0 \rightarrow S_{14}$	1.834	0.0047	241→247 (85)
G	2.28	$S_0 \rightarrow S_{15}$	1.908	0.0047	244→249 (86)
		$S_0 \rightarrow S_{16}$	1.958	0.0027	240→247 (70)
					245→250 (20)
H	2.47	$S_0 \rightarrow S_{20}$	2.067	0.0065	242→249 (29)
					238→247 (25)
					245→250 (21)
					240→247 (12)
		$S_0 \rightarrow S_{21}$	2.095	0.0068	246→251 (48)
					241→248 (12)
					236→247 (10)
		$S_0 \rightarrow S_{22}$	2.107	0.0043	242→249 (61)
					245→250 (17)
		$S_0 \rightarrow S_{23}$	2.108	0.0050	241→248 (56)
					246→251 (16)
					239→247 (10)

[a] S_0 denotes the ground state, while S_n denotes the nth excited state [b] Oscillator strength; only the most intense transitions are listed. [c] Molecular orbitals are denoted by their numbers (in this notation, HOMO and LUMO are 246 and 247, respectively), contributions less than 10% are omitted.

Vibrational spectroscopy: Isolation of isomerically pure $C_2(3)$-C_{82} in appreciable amounts enables its further characterization by vibrational spectroscopy, which, to our knowledge, has not yet been reported. Kikuchi et al. reported an IR spectrum of the mixture of $C_2(3)$-C_{82} with other unidentified isomers,[17] while the only Raman spectrum reported so far for C_{82} was the spectrum of the sample comprising two unidentified C_2 isomers in about a 1:1 ratio.[18] Figure 3 shows the FTIR and Raman (514 nm excitation) spectra of $C_2(3)$-C_{82} along with the wavenumbers of the most prominent peaks. Due to the strong fluorescence background, an acceptable signal-to-noise ratio in the Raman spectrum was obtained only with an excitation of 514 nm at a temperature of 5 K. As could be expected on the basis of the low molecular symmetry (which forces all 240 normal modes of $C_2(3)$-C_{82} to be both IR and Raman active), the spectra are very complex with a quasi-continuous distribution of the peaks in the whole range covering the fundamental vibrations of fullerenes (about 200–1650 cm^{-1}). Because of the different resonance conditions, the Raman spectrum measured in this work is substantially different from that reported by Eisler et al.;[18] however, the breathing mode (at 421 cm^{-1}) as well as the multiplet arising from the squashing mode (209–240 cm^{-1}) can be identified at almost the same positions as in the spectrum of the mixture of two C_2 isomers (note that the frequency of the breathing mode of the fullerenes was proved to be independent of the isomeric structure and scaled as the inverse root of the fullerene's molecular mass[18]). Significantly, though there is no inversion center in

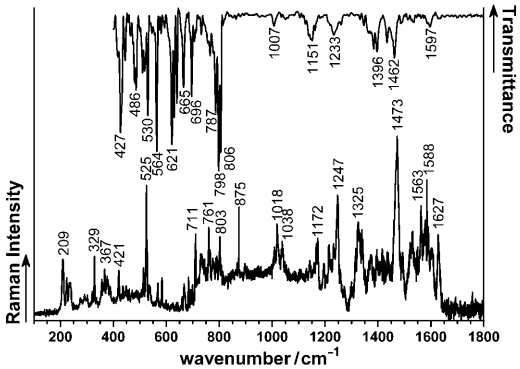

Figure 3. FTIR (KBr substrate, room temperature) and Raman (λ_{ex} = 514 nm, 5 K) spectra of $C_2(3)$-C_{82}.

$C_2(3)$-C_{82}, the almost spherical shape of the fullerenes results in the approximate fulfillment of the mutual exclusion rule. That is, strong IR bands have no intense counterparts in the Raman spectrum and vice versa.

Cyclic voltammetry: Electrochemical data evaluated from the cyclic voltammetry (CV) of the $C_2(3)$-C_{82} fullerene in *o*-DCB/TBAPF$_6$ (TBAPF$_6$ = tetrabutylammonium hexafluorophosphate) are summarized in Table 2. Four reversible reduction steps and two oxidation steps were detected.[10] The half-wave ($E_{1/2}$) potentials of the second, third, and fourth reduction steps as well as that of the first oxidation step are almost identical to those observed by Suzuki et al.,[19] except for a slightly more negative half-wave potential of −0.72 V versus ferrocene/ferrocenium (Fc/Fc$^+$) for the first reduction step observed in this work as compared to −0.69 V versus Fc/Fc$^+$ reported in reference [19]. Note that Burbank et al.[20] reported a different set of reduction potentials for C_{82} in pyridine, which are systematically shifted to the cathodic range by about 0.1–0.2 V (Table 2). In addition to the first oxidation peak, a second oxidation step at $E_{1/2} \cong 1.15$ V versus Fc/Fc$^+$ close to the edge of the potential window available was detected.[10] Concerning the recently detailed electrochemical studies of C_{82} and C_{84} empty fullerenes and the variety of $M_n@C_{82}$ and metallofullerenes performed by Anderson et al.,[21] the $C_2(3)$-C_{82} isomer can be attributed to the electrochemical class of empty fullerenes, in which a substantial gap between the second and third reduction step appears. Although no clear relationship between the electronic structures of metallofullerenes and the corresponding empty cages was observed in the recent square-wave voltammetric experiments,[21] it should be noted that the exact cage symmetry of all materials compared in the literature is still not known and in many cases the symmetry was not exactly proved by additional spectroscopic techniques.

Table 2. Redox potentials of $C_2(3)$-C_{82} fullerene.

Solvent/electrolyte (electrochemical method)[a]	$E_{1/2,ox(2)}$	$E_{1/2,ox(1)}$	$E_{1/2,red(1)}$	$E_{1/2,red(2)}$	$E_{1/2,red(3)}$	$E_{1/2,red(4)}$	$\Delta E_{gap,ec}$ [V]
o-DCB/TBAPF$_6$ (CV)	1.15	0.72	−0.72	−1.03	−1.58	−1.94	1.44
o-DCB/TBAPF$_6$ (CV)[b]	–	0.72	−0.69	−1.04	−1.58	−1.94	1.41
pyridine/TBAClO$_4$ (SWV)[c]	–	–	−0.47	−0.80	−1.42	−1.84	–

[a] CV = cyclic voltammetry, SWV = square-wave voltammetry. [b] Reference [19]. [c] Reference [20].

ESR spectra of the charged $C_2(3)$-C_{82} states: Reduction of C_{82} to its monoanion provided the radical state of the $C_{82}^{\bullet-}$ monoanion and is reported in detail elsewhere.[10] Briefly, the ESR spectra detected during the reduction of C_{82} in the potential region of the first reduction step (see also Figure 4, and 5, bottom inset) gave a very sharp and intense central ESR line ($\Delta B_{pp} = 0.15$ G) with a *g* factor of 2.0009, accompanied with ^{13}C satellites. Only one contribution by other groups to the ESR spectra of the reduced C_{82} was found in the literature. Fujitsuka et al.[13] detected a hint of a narrow ESR line of the reduced C_{82} fullerene solution with a weak signal at $g = 2.0021$, which was strongly overlapped by the signal of the TDAE$^{\bullet+}$ (TDAE = tetrakisdimethylamino ethylene) ion. Our spectroelectrochemical experiments proved the formation of the stable $C_2(3)$-C_{82} monoanion after reduction. Here, no interference with chemical reducing agents occurs and, consequently, well-defined ESR spectra could be observed.

Our spectroelectrochemical studies were further focused on the monitoring of the ESR response of multiply charged $C_2(3)$-C_{82}. At more negative potentials, including the second reduction step, the intensity of the ESR signal of C_{82}^- decreased (Figure 4, bottom) due to the reduction of the monoanion, and no new ESR signal was observed. This experiment confirms the diamagnetic character of the dianion formed. During the back scan, the intensity of the ESR signal increased after the reoxidation of the dianion to the monoanion. The nonzero intensity of the

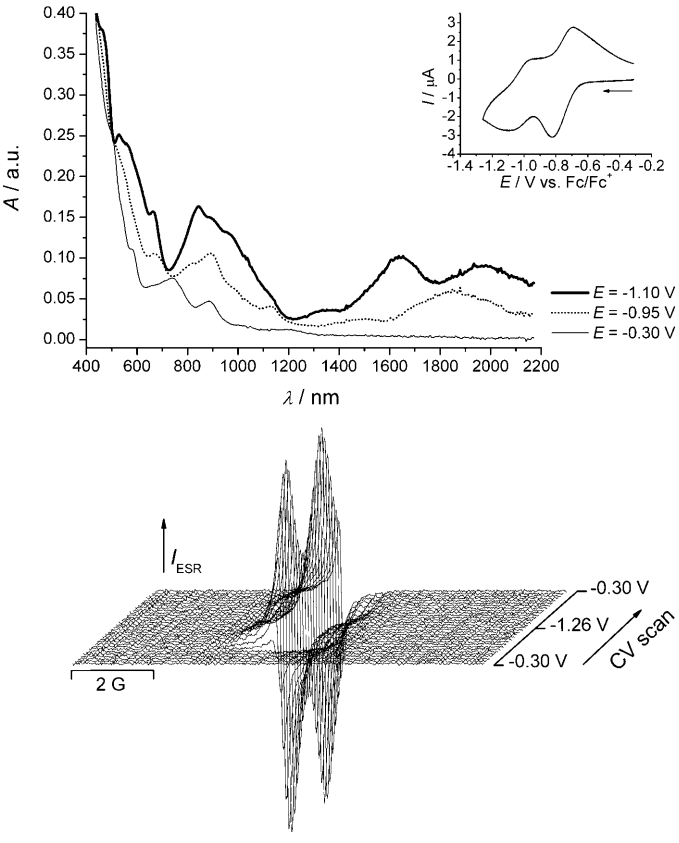

Figure 4. Top: Vis/NIR spectra of $C_2(3)$-C_{82} (——) and its anions detected during in situ spectroelectrochemistry in the potential region of the first (·····) and the second (——) reduction step; inset: cyclic voltammogram of this isomer in 0.2 M TBAPF$_6$/oDCB, scan rate = 3 mV s^{-1}. Bottom: the potential dependence of the ESR spectra of C_{82}^- in the potential region of the first and second reduction step.

ESR signal at the potentials of the second reduction step can easily be explained by the synproportionation reaction $C_{82}^{2-} + C_{82} \rightleftarrows 2\,C_{82}^{-}$, which evidently occurs in the bulk solution in the potential region of the second electron transfer, and by diffusion of the radical anion to the bulk solution away from the electrode surface so that it is still detectable by ESR.

During the reduction of the $C_2(3)$-C_{82} isomer in the potential region of the third reduction step, a new ESR signal with a g factor of 2.0020 and a line width $\Delta B_{pp} = 0.17$ G appeared (Figure 5, bottom; see also inset). This new signal can be assigned to the trianion $C_{82}^{\bullet 3-}$. This ESR signal appears at the third reduction step and disappears in the back scan under reoxidation in the cyclovoltammetric experiment (Figure 5, bottom). As the monoanion diffuses into the bulk solution, its signal is still present in the ESR spectrum, albeit to a low extent. However, by subtracting the monoanion signal, we gained the ESR spectrum of the C_{82} trianion characterized by a single sharp line, similar to that of the monoanion signal, but with a completely different ^{13}C satellite pattern and a strongly shifted g value. At even more negative electrode potentials, including also the fourth reduction step, a decrease of the $C_{82}^{\bullet 3-}$ ESR signal is observed and no new ESR signals occurred (Figure 5, bottom). Therefore, similar to the dianion, the tetraanion of the C_{82} fullerene is diamagnetic and ESR silent.

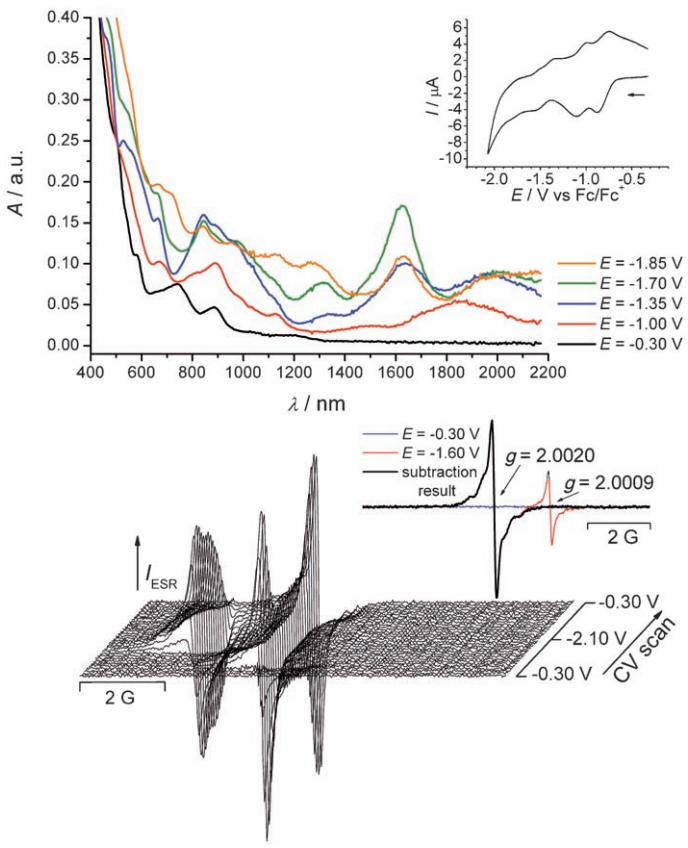

Figure 5. Top: Vis/NIR spectra of $C_2(3)$-C_{82} (black line) and its anions detected during in situ spectroelectrochemistry in the potential region of the first (red line), second (blue line), third (green line) and fourth (orange line) reduction step, inset: cyclic voltammogram (0.2 M $TBAPF_6$/oDCB, scan rate = 4.5 mV s^{-1}). Bottom: the potential dependence of ESR spectra of $C_{82}^{\bullet -}$ and $C_{82}^{\bullet 3-}$ in the potential region of the first, second, third, and fourth reduction step, inset: ESR spectrum of $C_{82}^{\bullet 3-}$ overlapped by the signal of $C_{82}^{\bullet -}$ (red line) detected during the reduction of $C_2(3)$-C_{82} at the potential of the third step, ESR spectrum of $C_{82}^{\bullet 3-}$ after subtraction of monoanion signal (black line).

An ESR signal was also observed in situ during the oxidation of the $C_2(3)$-C_{82} in the potential range of the first oxidation peak. As shown very recently,[10] we observed for the first time this stable cation of the empty fullerene at room temperature in a non-acidic medium. Similar to the monoanion and the trianion, a very sharp ESR line width $\Delta B_{pp} = 0.13$ G and additional ^{13}C satellites were observed. The g value (2.0029) of the cation is even larger than that of the trianion and the ^{13}C satellite pattern is significantly different for both mono- and trianion ESR signals. The different spin distribution of the cage depending on the charge of the species is discussed in the next section.

Spin density distribution in C_{82} radical ions: It is now established that radical anions of C_{60} and C_{70} exhibit broad ESR signals due to the degeneracy of the LUMOs in these fullerenes, which result in the close energies of the singly occupied molecular orbital (SOMO) and the next vacant orbital in respective anions (see reference [8] for a review). The small splitting of the molecular orbital (MO) levels results in a fast spin-lattice relaxation and a respective broadening of the ESR signal, while the spin-orbit coupling from unquenched angular momentum results in low g values. In contrast, as there is no symmetry-driven or accidental degeneracy of the LUMO energies in $C_2(3)$-C_{82}, the spectra of all charged paramagnetic states of C_{82} exhibit sharp ESR features. Furthermore, there is no Jahn–Teller distortion of C_2-C_{82} in the charged state, and hence the C_2 symmetry is expected for all charged states of C_{82}. In such a situation, the spin density in the cation, anion, and trianion reflects the HOMO, LUMO, and LUMO+1 orbital densities, respectively, of the neutral molecule, and, hence, it is no wonder that the ^{13}C patterns are different for $C_{82}^{\bullet +}$, $C_{82}^{\bullet -}$, and $C_{82}^{\bullet 3-}$.

To gain further insight into the electronic structure of the charged states of C_{82}, we have performed a series of DFT calculations. First, the structures of all charged states from +1 to −4 were optimized at the PBE/TZ2P level. Though the symmetry was not fixed in these calculations, optimization resulted in C_2 symmetric structures for all charged states. The calculations have also shown that the separation between frontier MO levels is sufficient to avoid the effects leading to the broadening of ESR lines in the radical anions of C_{60} and C_{70}.

For the analysis of the spin density distribution and ESR parameters, we employed the hybrid B3LYP functional because hybrid functionals are known to provide a more accurate description of these quantities.[22] Unfortunately, the large size and low symmetry of C_{82} preclude the use of the large basis sets necessary for an accurate prediction of hyperfine constants (hfcs), and calculations were performed

with the use of the relatively moderate but computationally efficient 6-311G* basis set. Figure 6a shows the B3LYP/6-311G* spin density distribution in radical ions, which is indeed found to vary considerably with the charge of the C_{82} fullerene. Figure 6b compares the distribution of the DFT predicted ^{13}C hfcs in C_{82}^{+}, C_{82}^{-}, and C_{82}^{3-}. Though the very high density of hfc values almost precludes a detailed assignment of the experimentally observed patterns (Figure 6c), the main experimental features are evidently reproduced and thus can be explained by computations. In agreement with the experimental spectrum, DFT predicts that the cation has the largest spread of ^{13}C hfcs ranging from −2 to +3 G. The feature marked A in the experimental spectrum of $C_{82}^{\bullet+}$ with hfc of about 3 G can be assigned to the C32 (C43) and C52 (C63) atoms, the DFT predicted hfcs of which are 2.778 G and 2.463 G (symmetry equivalent atoms are listed in parentheses; see Figure 6d for the labeling of the atoms). The tentative assignments of the features B and C with hfcs of about 1.2–1.8 and 1 G, respectively, are shown in Figure 6b. In general, having the largest spread of hfcs, $C_{82}^{\bullet+}$ also exhibits the most resolved ^{13}C satellite structure, which is in line with the comparably sparse distribution of its hfcs predicted by theory. In contrast to the cation, the anion has a much smaller range of hfcs (−1.5 to +1.5 G) and the least resolved ESR spectrum, which agrees with the almost Gaussian-type distribution of hfcs predicted by theory. That is, the largest density distribution is predicted close to zero, and the distribution is rather dense so that no prominent features can be distinguished in the ESR spectrum. Only the feature A′ can be tentatively assigned to the group of atoms C55 (C66), C54 (C65), C7 (C15), C1 (C4), C70 (C77), and C8 (C16) with DFT predicted hfcs of 1.514, −1.458, 1.243, −1.221, 1.218, and −1.191 G, respectively. The trianion has a similar spread of hfcs as the monoanion, but the shape of the distribution is different. Most importantly, the largest density of hfcs is expected at about −0.5 to −1.0 G, which results in a better resolved ESR spectrum with a clearly distinguished shoulder (marked B″) assigned to this maximum in hfc distribution. Assignment of the other experimental feature, A″, is also quite clear from the analysis of the distribution of hfc values (Figure 6b).

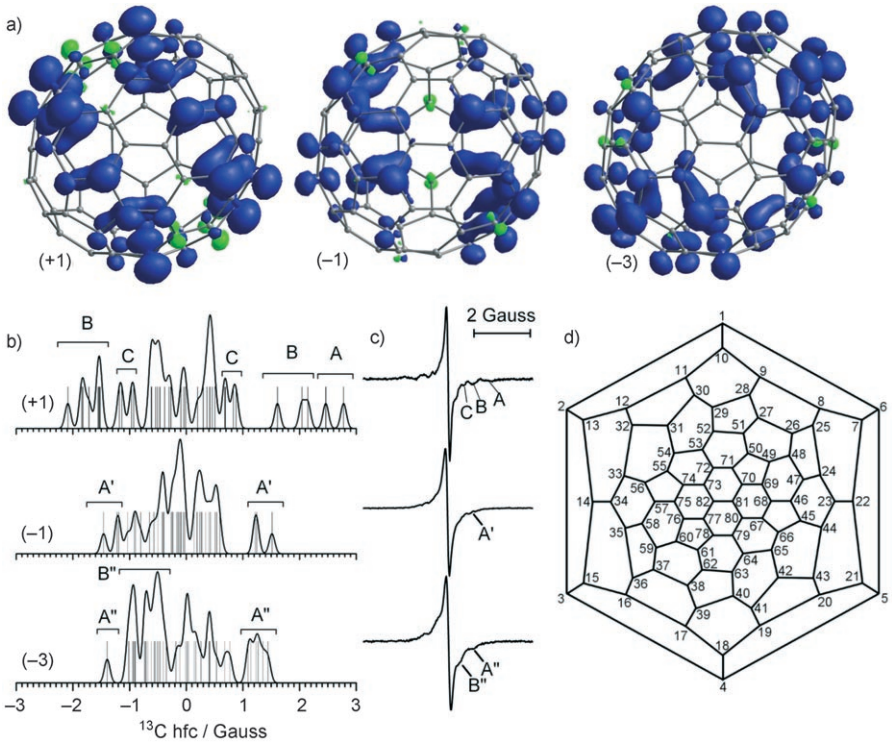

Figure 6. a) Spatial distribution of spin density (+ blue, − green); b) distribution of ^{13}C hfcs in respective ions (bars represent individual hfc values, curves correspond to their broadening by the Gaussian function with a half-width of 0.1 G); c) ESR spectra of C_{82} radical-ions (for the sake of comparison, the spectra were shifted in the magnetic field scale); d) Schlegel diagram of $C_2(3)$-C_{82} with IUPAC numbering schema.

Vis/NIR spectra of the charged states of C_{82}: As most of the endohedrals consist of negatively charged cages and positively charged encapsulated units, the Vis/NIR spectroscopic characteristics of charged, empty C_{82} isomers are highly interesting. Therefore, we performed in situ Vis/NIR spectroelectrochemical experiments on the $C_2(3)$-C_{82} isomer to measure the characteristic optical bands of the $C_2(3)$-C_{82} isomer in different negatively as well as positively charged states.

The reduction of $C_2(3)$-C_{82} in the first step causes the appearance of well-defined Vis/NIR bands with maxima at 670, 890, 1135, and 1850 nm (Figure 4, top). As the intensity changes of these bands correlate well with the rise and decrease of the ESR signal during the voltammetric cycle, they can be unambiguously assigned to the $C_2(3)$-C_{82} monoanion (see Supporting Information).

New absorption maxima at 843, 1637, and 1980 nm were detected in the Vis/NIR spectra when the potential scan was extended to the second reduction step (Figure 4, top). These bands can be assigned to the C_{82} dianion due to the correlation of their intensities with the charge transferred in the second reduction step. As already observed in the ESR spectroelectrochemistry, a minor component of the C_{82} monoanion is still observable in the second electron transfer due to its diffusion into the bulk solution.

An increase of the two absorption maxima at 1322 and 1621 nm was observed at the potential of the third reduction step, and the band of the dianion at 843 nm decreases at this potential (Figure 5, top). The new bands can be assigned to the trianion $C_{82}^{\bullet 3-}$, even though the small absorption around 1322 nm was already observed in the spectra of the dianion. The maximum at 1621 nm overlaps strongly with the dianion band at 1637 nm. However, the strong increase in the intensity in comparison to the dianion spectra points to the formation of a new species ($C_{82}^{\bullet 3-}$) rather than the accumulation of the C_{82}^{2-}. Moreover, the changes in the overlapping bands (1322 and 1621 nm) correlate well with the change in the ESR spectra of $C_{82}^{\bullet 3-}$. Moving to even more negative potentials, including the fourth reduction step, the decrease of the most intense trianion band at 1621 nm was observed and two new bands of a tetraanion with maxima at 725 and 1145 nm emerged (Figure 5, top).

Two absorption maxima at 890 and 1995 nm were detected during the oxidation of the C_{82} isomer under study in the first oxidation step, as already reported elsewhere by our group.[10] Their intensities correlate well with the intensity of the simultaneously monitored ESR line (see Supporting Information). Therefore, they can be clearly assigned to the C_{82} radical cation. The stability of the C_{82} cations is lower than that of the anions. At potentials of the second oxidation peak in the voltammetric experiment, the working electrode started to be covered by a film and a distortion of the baseline in the Vis/NIR spectra occurs. This yet unidentified reaction that forms the film at the electrode hindered our attempts to observe Vis/NIR signals of the dication of the C_{82} fullerene.

Conclusion

In this work, the separation procedure and detailed spectroscopic and spectroelectrochemical characterization of the major isomer of the C_{82} fullerene is given. The results of our study, including Vis/NIR spectra and TD-DFT calculations, confirm the assignment of the structure of this fullerene to the $C_2(3)$-C_{82} isomer. The vibrational spectra (both IR and Raman) of $C_2(3)$-C_{82} are given for the first time in detail. Special efforts were devoted to the generation and characterization of the charged states of $C_2(3)$-C_{82}, and, thus, spectroscopic information on the charged C_{82} from $+1$ to -4 are now available. These data include Vis/NIR absorption spectra of all electrochemically generated charged states of C_{82} as well as ESR spectra of $C_{82}^{\bullet +}$, $C_{82}^{\bullet -}$, and $C_{82}^{\bullet 3-}$ paramagnetic fullerene ions. We have found remarkable differences in the ^{13}C satellites pattern of the $C_{82}^{\bullet +}$, $C_{82}^{\bullet -}$, and $C_{82}^{\bullet 3-}$ radicals. Variations of the spectra with charge were rationalized by DFT calculations, and a tentative assignment of the most prominent features in the spectra is provided.

Experimental Section

Synthesis and HPLC separation: As a starting material, the soot of the arc synthesis of endohedral fullerenes (preferably for lanthanum, but also for cerium, yttrium and samarium) was used as synthesized according to Krätschmer and Huffman process using graphite rods and a metal/graphite powder mixture.[23] Two fractions of the soot containing as the main products C_{80} and C_{84}, respectively, were collected by preparative HPLC (Gilson, USA) using a Buckyprep column, 20x250 mm (Nacalai Tesque, Japan) at room temperature at a flow rate of 10 mL min^{-1} with toluene as the eluent. The second separation step on an analytical HPLC (Agilent 1100, USA) was done with two analytical Buckyprep columns 4,6x250 mm (Nacalai Tesque, Japan) in a row at a temperature of 40 °C and a flow rate of 1.6 mL min^{-1} with toluene as an eluent. The final separation was done by recycling HPLC (SunChrom, Germany) at a 5PYE column 10x250 mm at room temperature, a flow rate of 5 mL min^{-1}, and toluene as an eluent.

Spectroscopic measurements: A laser desorption ionization (LDI) time-of-fight (TOF) Biflex 3 spectrometer (Bruker, Germany) and both negative and positive ion detection modes were used throughout for the characterization of the fullerenes. No matrix was applied for the laser ionization of the fullerenes. The ^{13}C NMR spectrum of the C_{82} isomer sample was recorded using a 500 MHz spectrometer (Avance II 500 MHz, Bruker, Germany). The sample (ca. 1 mg) was dissolved in CS_2 (0.4 mL), a coaxial capillary tube filled with [D_6]acetone was used as an external lock. The cap of the NMR tube was wrapped with Teflon tape and spectra were recorded at 288 K to minimize the evaporation of the solvent during the measurement. Absorption spectra of the sample were measured using UV/Vis/NIR 3101-PC spectrometer (Shimadzu, Japan). FTIR spectra were measured by using a IFS-66v spectrometer (Bruker) with a resolution of 2 cm^{-1}. The sample dissolved in toluene (1 mL) was drop-coated onto a single crystal KBr disk. Residual solvent was removed by heating the film in vacuo at 498 K for 3 h. The Raman spectrum was measured using a T64000 triple monochromator spectrometer (Jobin Yvon, France). The spectrum was excited by the 514.5 nm line of Ar^+ laser (Innova 300 series, Coherent, USA). The sample was drop-coated on a copper substrate and cooled to 5 K.

Spectroelectrochemical measurements: For a typical electrochemical and spectroelectrochemical study, C_{82} dissolved in toluene was dried, transported to a glove box (oxygen and water content below 1 ppm), and immediately redissolved in 1,2-dichlorobenzene (*o*-DCB, anhydrous, 99%, Aldrich) with the concentration ranging from 1×10^{-4} to 5×10^{-4} mol L^{-1}. Tetrabutylammonium hexafluorophosphate (TBAPF$_6$, Fluka, dried under reduced pressure at 340 K for 24 h prior to use) was then added as the supporting electrolyte with a concentration of 0.1–0.2 mol L^{-1}. The cyclic voltammogram was obtained in a glove box with a PAR 273 potentiostat (EG&G, USA) in a three-electrode system, with platinum wires as working and counter electrodes and a silver wire as a pseudo-reference electrode. Ferrocene (Fc) was added as the internal standard after each measurement and all potentials are corrected versus the Fc/Fc^+ couple. A PG 284 potentiostat (HEKA, Germany) was used as electrochemical equipment in the in situ ESR/UV/Vis/NIR spectroelectrochemical studies. ESR spectra were recorded on an EMX X-Band ESR spectrometer (Bruker, Germany), and optical spectra were obtained by the UV/Vis/NIR spectrometer system TIDAS (J&M, Germany).

DFT calculations: Geometry optimization of C_{82} and its charged states was performed using PBE functional[24] and the PRIRODA quantum chemical code.[25,26] The code employed the expansion of the electron density in an auxiliary basis set to accelerate evaluation of the Coulomb and exchange correlation terms,[25] no symmetry constraints were adopted. Point-energy calculations at the B3LYP/6-311G* level of theory were performed with the use of PC GAMESS.[27]

Acknowledgements

Financial support of the Deutsche Forschungsgemeinschaft is gratefully acknowledged. Financial support for P.R. by the Alexander von Humboldt Foundation (Project 3 Fokoop DEU/1063827) and the Slovak Scientific Grant Agency (1/3579/06) is also duly acknowledged. A.P. thanks DAAD and CRDF (Award RUC2–2830-MO-06). We cordially thank K. Leger, S. Schiemenz and F. Ziegs for technical assistance.

[1] P. Fowler, D. E. Manolopoulos, *An Atlas of Fullerenes*, Clarendon, Oxford (UK), **1995**.
[2] H. Shinohara, *Rep. Prog. Phys.* **2000**, *63*, 843–892.
[3] T. Akasaka, H. Nagase in *Endofullerenes: A New Family of Carbon Clusters*, Kluwer, Dordrecht, **2002**.
[4] L. Dunsch, S. Yang, *Electrochem. Soc. Interface* **2006**, *15*, 34–38.
[5] S. Guha, K. Nakamoto, *Coord. Chem. Rev.* **2005**, *249*, 1111–1132.
[6] M. Krause, M. Hulman, H. Kuzmany, P. Kuran, L. Dunsch, T. J. S. Dennis, M. Inakuma, H. Shinohara, *J. Mol. Struct.* **2000**, *521*, 325–340.
[7] T. Kodama, N. Ozawa, Y. Miyake, K. Sakaguchi, H. Nishikawa, I. Ikemoto, K. Kikuchi, Y. Achiba, *J. Am. Chem. Soc.* **2002**, *124*, 1452–1455.
[8] C. A. Reed and R. D. Bolskar, *Chem. Rev.* **2000**, *100*, 1075–1119.
[9] P. Rapta, A. Bartl, A. Gromov, A. Stasko, L. Dunsch, *ChemPhysChem* **2002**, *3*, 351–356.
[10] M. Zalibera, P. Rapta, L. Dunsch, *Electrochem. Commun.* **2007**, *9*, 2843–2847.
[11] K. Kikuchi, N. Nakahara, T. Wakabayashi, S. Suzuki, H. Shiromaru, Y. Miyake, K. Saito, I. Ikemoto, M. Kainosho, Y. Achiba, *Nature* **1992**, *357*, 142–145.
[12] K. Kikuchi, N. Nakahara, T. Wakabayashi, M. Honda, H. Matsumiya, T. Moriwaki, S. Suzuki, H. Shiromaru, K. Saito, K. Yamauchi, I. Ikemoto, Y. Achiba, *Chem. Phys. Lett.* **1992**, *188*, 177–180.
[13] M. Fujitsuka, A. Watanabe, O. Ito, K. Yamamoto, H. Funasaka, T. Akasaka, *J. Phys. Chem. B* **1999**, *103*, 9519–9523.
[14] G. Y. Sun, M. Kertesz, *J. Phys. Chem. A* **2001**, *105*, 5468–5472.
[15] B. Gao, L. Liu, C. R. Wang, Z. Y. Wu, Y. Luo, *J. Chem. Phys.* **2007**, *127*, 164314.
[16] R. Bauernschmitt, R. Ahlrichs, F. H. Hennrich, M. M. Kappes, *J. Am. Chem. Soc.* **1998**, *120*, 5052–5059.
[17] K. Kikuchi, S. Suzuki, Y. Nakao, N. Nakahara, T. Wakabayashi, H. Shiromaru, K. Saito, I. Ikemoto, Y. Achiba, *Chem. Phys. Lett.* **1993**, *216*, 67–71.
[18] H. J. Eisler, S. Gilb, F. H. Hennrich, M. M. Kappes, *J. Phys. Chem. A* **2000**, *104*, 1762–1768.
[19] T. Suzuki, K. Kikuchi, F. Oguri, Y. Nakao, S. Suzuki, Y. Achiba, K. Yamamoto, H. Funasaka, T. Takahashi, *Tetrahedron* **1996**, *52*, 4973–4982.
[20] P. B. Burbank, J. R. Gibson, H. C. Dom, M. R. Anderson, *J. Electroanal. Chem.* **1996**, *417*, 1–4.
[21] M. R. Anderson, H. C. Dorn, S. A. Stevenson, *Carbon* **2000**, *38*, 1663–1670.
[22] M. Munzarova in *DFT Calculations of EPR Hyperfine Coupling Tensors* (Eds.: M. Kaupp, M. Buhl, V. G. Malkin), Wiley-VCH, Weinheim, **2004**, pp. 463–472.
[23] L. Dunsch, A. Bartl, P. Georgi, P. Kuran, *Synth. Met.* **2001**, *121*, 1113–1114.
[24] J. P. Perdew, K. Burke, M. Ernzerhof, *Phys. Rev. Lett.* **1996**, *77*, 3865–3868.
[25] D. N. Laikov, *Chem. Phys. Lett.* **1997**, *281*, 151–156.
[26] D. N. Laikov, Y. A. Ustynuk, *Russ. Chem. Bull.* **2005**, *54*, 820–826.
[27] A. A. Granovsky in PC GAMESS, version 7.15, URL: http://classic.chem.msu.su/gran/gamess/index.html, Vol. **2008**.

Received: March 31, 2008
Revised: June 22, 2008
Published online: September 18, 2008

